In vivo chemical exchange saturation transfer imaging allows early detection of a therapeutic response in glioblastoma

Koji Sagiyama[a,1], Tomoyuki Mashimo[b,c,1], Osamu Togao[a], Vamsidhara Vemireddy[c,d], Kimmo J. Hatanpaa[e], Elizabeth A. Maher[b,c,d], Bruce E. Mickey[f], Edward Pan[c,d], A. Dean Sherry[a,g], Robert M. Bachoo[b,c,d,2], and Masaya Takahashi[a,g,2]

[a]Advanced Imaging Research Center, [b]Department of Internal Medicine, [c]Harold C. Simmons Comprehensive Cancer Center, and Departments of [d]Neurology and Neurotherapeutics, [e]Pathology, [f]Neurosurgery, and [g]Radiology, University of Texas Southwestern Medical Center, Dallas, TX 75390

Edited by Adriaan Bax, National Institutes of Health, Bethesda, MD, and approved February 19, 2014 (received for review December 21, 2013)

Glioblastoma multiforme (GBM), which account for more than 50% of all gliomas, is among the deadliest of all human cancers. Given the dismal prognosis of GBM, it would be advantageous to identify early biomarkers of a response to therapy to avoid continuing ineffective treatments and to initiate other therapeutic strategies. The present in vivo longitudinal study in an orthotopic mouse model demonstrates quantitative assessment of early treatment response during short-term chemotherapy with temozolomide (TMZ) by amide proton transfer (APT) imaging. In a GBM line, only one course of TMZ (3 d exposure and 4 d rest) at a dose of 80 mg/kg resulted in substantial reduction in APT signal compared with untreated control animals, in which the APT signal continued to increase. Although there were no detectable differences in tumor volume, cell density, or apoptosis rate between groups, levels of Ki67 (index of cell proliferation) were substantially reduced in treated tumors. In another TMZ-resistant GBM line, the APT signal and levels of Ki67 increased despite the same course of TMZ treatment. As metabolite changes are known to occur early in the time course of chemotherapy and precede morphologic changes, these results suggest that the APT signal in glioma may be a useful functional biomarker of treatment response or degree of tumor progression. Thus, APT imaging may serve as a sensitive biomarker of early treatment response and could potentially replace invasive biopsies to provide a definitive diagnosis. This would have a major impact on the clinical management of patients with glioma.

molecular MRI | chemical exchange transfer imaging | chemoresistance

Glioblastoma multiformes (GBMs) account for more than 50% of all gliomas, and are among the deadliest of all human cancers. Approximately 10,000 patients in the United States are diagnosed each year with GBM, and the median survival time remains at 15 mo despite recent advances in surgery, radiation therapy, and chemotherapy (1). During the past two decades, our knowledge of the aberrant molecular mechanisms that underlie gliomas has increased extensively (2); however, advancement in the treatment of glioma has lagged far behind that in other cancers, except for significant progress made by the introduction of temozolomide (TMZ) (3, 4). TMZ, an oral alkylating chemotherapeutic agent, disturbs DNA replication and induces apoptosis of cancer cells, and subsequently arrests progression of the tumor. For these reasons, TMZ has been widely adopted as standard-of-care treatment for GBM (1, 5). Although TMZ can significantly prolong survival on average, only 45% of patients with newly diagnosed GBM gain substantial benefits from TMZ (6). Furthermore, even in cases in which the tumor responds well to initial treatment and appears to have disappeared on follow-up, recurrence is common and fatal in the middle of treatment or 1–2 y after completion of the treatment in most cases (7, 8).

The prognosis and management is vastly different depending on whether one observes tumor progression or treatment effects. Thus, it is critical to decide whether the treatment should be continued or switched to avoid continuing ineffective treatments. Currently, management decisions in all phases of diagnosis, treatment and follow-up rely on MRI (9–11). Generally, clinicians make a decision based on interpretation of signal changes in T2-weighted (T2W) or fluid-attenuated inversion recovery and gadolinium enhancement on T1-weighted (T1W) imaging from one time point to another, typically covering several months. In addition, patients are taken back to the operating room for a repeat craniotomy and biopsy to make the confirmative diagnosis, as the currently available imaging methods often do not suffice to make the final decision. Thus, overall, there is an urgent need for the development of novel imaging techniques that can differentiate between continued progression vs. a positive response to therapy at these critical decision points as early and accurate as possible.

Chemical exchange transfer (CEST) has drawn considerable attention as a novel mechanism of MRI contrast. This method provides more detailed physiological and functional information than conventional MRI and has emerged in the field of molecular imaging (12, 13). CEST contrast is achieved by applying a presaturation pulse at the resonance frequency of a slow–intermediate exchanging proton site (−NH, −OH, or metal-bound water molecule) of endogenous or exogenous agents.

Significance

The prognosis and management of patients with glioma is vastly different depending on whether one detects tumor progression or treatment effects. Although the gold standard in the evaluation of treatment efficacy involves MRI, the currently available imaging methods often do not suffice to make the final decision. Our study demonstrated that amide proton transfer (APT) imaging, one subset of chemical exchange saturation transfer imaging, can detect molecular signals in glioma induced by short-term chemotherapy with temozolomide. These molecular events precede morphologic changes. The APT signal did not decrease in tumors resistant to chemotherapy. APT imaging may provide a useful prognostic biomarker of treatment response or tumor progression in glioma.

Author contributions: K.S., T.M., E.A.M., A.D.S., R.M.B., and M.T. designed research; K.S., T.M., O.T., V.V., K.J.H., B.E.M., E.P., and M.T. performed research; K.S., T.M., O.T., V.V., and K.J.H. analyzed data; and K.S., T.M., A.D.S., R.M.B., and M.T. wrote the paper.

The authors declare no conflict of interest.

This article is a PNAS Direct Submission.

[1]K.S. and T.M. contributed equally to this work.

[2]To whom correspondence may be addressed. E-mail: robert.bachoo@utsouthwestern.edu or masaya.takahashi@utsouthwestern.edu.

This article contains supporting information online at www.pnas.org/lookup/suppl/doi:10.1073/pnas.1323855111/-/DCSupplemental.

www.pnas.org/cgi/doi/10.1073/pnas.1323855111

The resulting saturated or partially saturated spin is transferred to bulk water via chemical exchange. Consequently, specific molecular information is obtained indirectly through the MRI signal of tissue water. The net effect of CEST is to reduce the bulk water signal intensity detected in an imaging experiment, thereby providing negative contrast (14).

Amide proton transfer (APT) imaging is one subset of CEST imaging that refers specifically to chemical exchange between protons of free tissue water (bulk water) and amide groups (−NH) of endogenous mobile proteins and peptides. It has been reported that such exchangeable protons are more abundant in tumor tissues than in healthy tissues (15). When applied to rats implanted with 9L gliosarcoma tumors in brain, APT imaging was able to distinguish between pathology-confirmed regions of tumor vs. tissue edema, whereas standard T1W, T2W, and fluid-attenuated inversion recovery imaging or diffusion-weighted imaging could not. Other previous reports demonstrated that the APT signal increased by 3–4% in tumor compared with peritumoral brain tissue in an experimental rat glial tumor at 4.7 T (16) and human brain tumor at 3 T (17). We recently demonstrated that APT imaging can distinguish histopathological World Health Organization grade of diffuse gliomas in patients (18). The mean APT signal increased with tumor grade (grade II, 2.1 ± 0.4%; III, 3.2 ± 0.9%; and IV, 4.1 ± 1.0%) and clearly discriminated between low-grade (i.e., grade II) and high-grade (i.e., grades III and IV) gliomas. Moreover, Zhou et al. clearly demonstrated in rat models that the method could distinguish tumor from radiation necrosis and further that the APT signal decreased in the tumor after radiation therapy (19). These previous studies indicate that APT imaging may be a more sensitive and specific biomarker for characterization of tumor grade or therapeutic response to radiation in brain tumors than other more conventional MRI methods.

Here, we demonstrate quantitative assessment of early treatment response in short-term chemotherapy with TMZ in vivo by APT imaging of brain gliomas. A validated noninvasive biomarker of progression or therapeutic response of glioblastoma in patients could potentially reduce the need for craniotomy and biopsy during and after chemotherapy in these patients. Among the imaging methods that potentially can be used for this purpose, APT imaging appears to be a most promising method for early detection of a therapeutic response.

Results

The human orthotopic tumor (HOT) mouse model of GBM (20) was used in these studies. Briefly, tumors were removed from patients during surgery, dissociated, and injected into the brain of a nonobese diabetic SCID mouse without exposure to tissue culture conditions. The mice develop tumors within ~3 mo, and the tumor is then passaged from one mouse to another without experiencing cell culture conditions. This model has been shown to faithfully recapitulate the histology, genetics, metabolic, and imaging features of the human tumor, even when taken through multiple passages in the mouse brain without adaption to cell culture (21).

Comparison Between With and Without Treatment in a GBM Line Responsive to TMZ Treatment (Experiment I). Eleven mice with a GBM line derived from a patient who had shown a response to TMZ treatment were used in the first experiment. Tumor growth in the brain was monitored by MRI using standard T2W imaging. When the tumors reached a size of 3–5 mm (~4–5 wk after implantation), the mice were divided into two groups such that the average diameter of the tumors was equal in each group (baseline). In the treated group ($n = 6$), the mice underwent one course of treatment of TMZ (80 mg/kg i.p. for 3 d and then rest for 4 d; 7 d total). The second untreated group served as control ($n = 5$). High-resolution T2W and APT images were collected on both groups of animals at baseline and 1 wk after initiating treatment with TMZ.

Human GBM growing in mouse brain appears hyperintense in high-resolution axial multislice T2W images (100-μm spatial resolution; Fig. 1*A*). The mean tumor volume was not different between the control and treated groups at baseline (27.52 ± 14.04 mm^3 vs. 30.59 ± 17.57 mm^3; $P = 0.76$). At 1 wk after initiating therapy, the tumor volumes were highly variable, so, again, a difference was not statistically detectable between the two groups (88.07 ± 55.95 mm^3 vs. 46.78 ± 26.46 mm^3; $P = 0.14$; Fig. 1*B*). The volume change (as a percentage) within 1 wk relative to baseline also showed no detectable difference between the control (241.5 ± 196.8%) and the treated (70.72 ± 117.0%; $P = 0.10$) groups. Although the volumes varied within each group, the tumor tended to grow more rapidly in the control group (Fig. 1*C*).

APT images were collected in a single 1-mm axial slice through the maximum diameter of each tumor. Normal, healthy brain tissue displayed negative and lower APT values compared with tumor at baseline and 1 wk (Fig. 2*A*, white arrow) as reported in previous literature (16). In all untreated control animals, the enhanced area increased drastically at 1 wk relative to baseline (7.97 ± 3.64 mm^2 vs. 19.26 ± 7.52 mm^2; $P < 0.05$; Fig. 2*B*), whereas there was no change in the area in the treated animals (9.17 ± 2.99 mm^2 vs. 8.77 ± 3.85 mm^2; $P = 0.87$). The differences in percentage change of the enhanced area within 1 wk relative to baseline showed no difference between the control (181.8 ± 168.1%) and the treated (11.75 ± 75.0%; $P = 0.052$) groups, although the tumor tended to grow more rapidly in the control group (Fig. 2*C*). Corrected APT ratio (APTR) in the tumor is normalized by APTR in the normal tissue on the APT weighted (APTW) image as follows: APTR in tumor subtracted by that in contralateral normal tissue. Hence, the corrected APTRs indicate "tissue contrast" between tumor and normal tissues on APTW images. Interobserver agreement for the measurement of corrected APTR between the two observers in 22 measurements ($n = 11$ for each at baseline and 1 wk) showed excellent agreement, with the intraclass correlation coefficient of 0.98 and r^2 of 0.99.

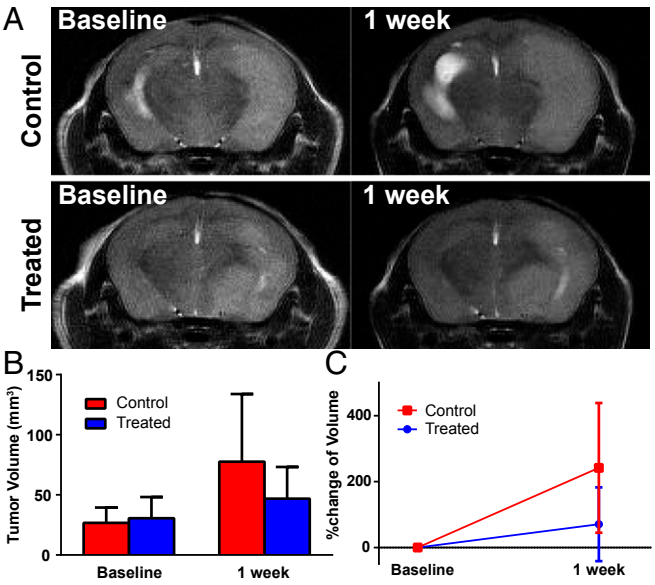

Fig. 1. Temporal change of glioblastoma on T2W images in the orthotopic mouse model with and without short-term TMZ treatment. (*A*) Typical axial T2W images of brain in the orthotopic mouse model with human GBMs in the control (*Upper*) and treated (*Lower*) groups at baseline (*Left*) and 1 wk after (*Right*). (*B*) Mean tumor volume measured on multislice T2W images in the control ($n = 5$) and treated ($n = 6$) groups. (*C*) Change (as a percentage) in volume at 1 wk relative to baseline. Data are presented as mean ± SD.

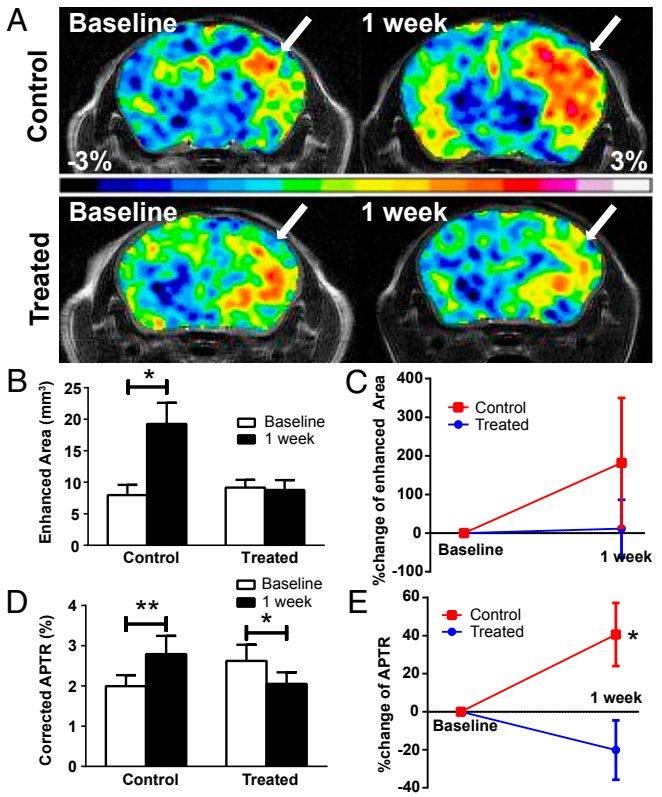

Fig. 2. Temporal change of glioblastoma on APTW images in the orthotopic mouse model with and without short-term TMZ treatment. (*A*) Typical axial APTW images of brain in the orthotopic mouse model with human GBMs in the control (*Upper*) and treated (*Lower*) groups at baseline (*Left*) and 1 wk after (*Right*). The imaging slabs correspond to those on T2W images in Fig. 1*A*. (*B*) Temporal change in the mean enhanced area measured on APTW images in the control ($n = 5$) and treated ($n = 6$) groups. (*C*) The change (as a percentage) in the enhanced area at 1 wk relative to baseline. (*D*) The corrected APTR (contrast between tumor and normal brain on APTW images) in control and treated groups. (*E*) The change (as a percentage) in the corrected APTR relative to baseline between the groups. Data represented as mean ± SD (*$P < 0.05$ and **$P < 0.01$).

In the untreated control group, the corrected APTR increased at 1 wk (2.79 ± 0.45%; $P < 0.01$) from baseline (1.99 ± 0.27%), whereas it decreased after chemotherapy (2.62 ± 0.40% vs. 2.05 ± 0.28%; $P < 0.05$) in the treated group (Fig. 2*D*). As a consequence, the differences in percentage change from baseline in the corrected APTR between the control (40.59 ± 16.63%) and the treatment (−20.14 ± 15.59%; $P < 0.001$) groups were significant (Fig. 2*E*). We tested whether the corrected APTR correlates with the tumor volume at baseline ($n = 11$) and found there was no significant correlation between the two parameters ($r^2 = 0.34$; $P = 0.06$).

To identify whether any microscopic morphological change could be detected, we prepared H&E staining of the slice corresponding to the slab imaged by APT. We observed several morphological alterations such as enlarged nucleus, cytoplasmic vacuolation, or foam cell changes in the tumors treated with four courses of TMZ in the same animal model, consistent with previous literature reports (22, 23); however, similar morphological changes were not found in any treated animals in this study (Fig. 3*A*). There were no differences in cell density between the control and treated groups (2,141 ± 501.0 /mm^2 vs. 1,963 ± 438.1 /mm^2; $P = 0.61$; Fig. 3*B*). Furthermore, a caspase-3 assay revealed that the percentage of apoptotic cells was low, and no differences were found between the control and treated groups (1.93 ± 0.47% vs. 1.45 ± 0.43%; $P = 0.18$; Fig. 3*C*).

Although it is known that TMZ induces apoptosis (3), one assumes that the short-term exposure (3 d) may not have been sufficient to induce such morphological changes associated with apoptosis within 1 wk in the GBM line. However, the Ki67 labeling index (Ki67LI; i.e., percentage of cells that appear Ki67-positive) was significantly lower in the treated group (8.03 ± 1.04%; $P < 0.0001$) compared with the control group (56.24 ± 8.42%; Fig. 3*D*). Ki67LI shows a correlation with the corrected APTR ($r^2 = 0.84$; $P < 0.01$; Fig. S1*A*). This correlation was also shown in each group (control, $r^2 = 0.83$; Fig. S1*B*; treated, $r^2 = 0.99$; Fig. S1*C*), although the sample size was small in these correlations.

Comparison Between Responsive and Resistant GBM Lines to TMZ Treatment (Experiment II). The first study design tested whether APT imaging can detect an early treatment response to short-term chemotherapy with TMZ but did not address treatment response (as measured by the APT signal) with long-term prognosis of the animals. Two matched tumor lines were isolated from a patient whose tumor recurred after having previously received standard therapy (concurrent radiation and TMZ followed by 12 cycles of TMZ). The first HOT GBM line was generated from the tumor at the time of initial resection from the patient who subsequently responded well to TMZ treatment. At the time of recurrence, the patient underwent a second resection, and a sample of tumor was used to generate a second HOT GBM line. As anticipated, the initial and recurrent tumor models were TMZ sensitive and resistant, respectively. Because genomic profiles of these initial and recurrent tumors from the same patient were remarkably similar (20), this in vivo model offers a unique and powerful system to compare directly the APT signal in the setting of TMZ sensitivity and resistance. Three mice from the initial tumor line and six from the recurrent tumor line underwent the same protocol of TMZ treatment (80 mg/kg i.p. for 3 d and then rest for 4 d; 7 d total) and APT imaging at baseline and 1 wk after initiating treatment with TMZ.

The mean tumor volume was not different between the initial and recurrent tumor groups at baseline (44.88 ± 12.84 mm^3 vs. 32.55 ± 7.52 mm^3; $P = 0.10$). One week after starting treatment,

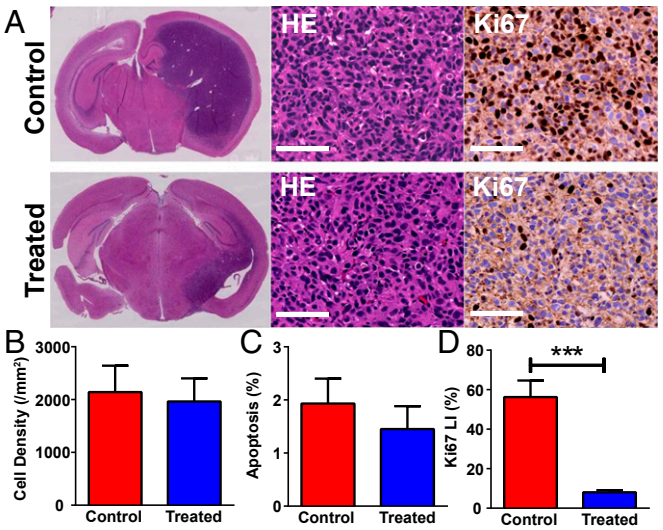

Fig. 3. Histological evaluation of the glioblastoma in the orthotopic mouse model with and without short-term TMZ treatment. (*A*) H&E staining on the slice corresponding to the image slabs on T2W (Fig. 1*A*) and APTW (Fig. 2*A*) imaging (*Left*), H&E staining (magnification, 20×; *Middle*), and Ki67 staining (magnification, 20×; *Right*) of the tumors. (Scale bars: 100 μm.) (*B*) Cell density between the two groups ($n = 4$ per group). (*C*) The percentage of cells showing apoptosis in the caspase-3 assay. (*D*) Ki67LI is the percentage of cells that are Ki67-positive. Data are presented as mean ± SD (***$P < 0.0001$).

the mean tumor volume was higher in the recurrent tumors (77.53 ± 14.64 mm^3; $P < 0.001$) than in the initial tumors (15.47 ± 7.90 mm^3). In response to treatment, the mean tumor volume increased in the recurrent tumors whereas that of the initial tumors decreased. Therefore, the volume change within 1 wk relative to baseline showed a difference between the initial tumors (−67.00 ± 7.88%) and the recurrent tumors (141.9 ± 34.37%; $P < 0.0001$). Fig. 4*A* demonstrates the typical APTW images at baseline and 1 wk after chemotherapy with TMZ. The recurrent tumor showed higher corrected APTR than the initial tumor before treatment (2.50 ± 0.21% vs. 2.18 ± 0.07%; $P < 0.05$). In all recurrent tumors, the enhanced area increased significantly at 1 wk relative to baseline (5.37 ± 1.56 mm^2 vs. 11.56 ± 2.97 mm^2; $P < 0.01$), whereas there was no significant change in the area in the initial tumors (5.60 ± 3.51 mm^2 vs. 2.30 ± 1.03 mm^2; $P = 0.14$). The percentage change in the APT-enhanced areas at 1 wk relative to baseline differed between the initial tumors (−58.08 ± 6.78%) and the recurrent tumors (129.7 ± 87.08%; $P < 0.01$). In the initial tumors, the corrected APTR decreased after chemotherapy (1.62 ± 0.12%; $P < 0.05$) from baseline (2.18 ± 0.07%), whereas it increased after chemotherapy (2.50 ± 0.21% vs. 3.45 ± 0.32%; $P < 0.01$) in the recurrent tumors. As a consequence, the differences in percentage change from baseline in the corrected APTR between the initial and recurrent tumors were significant (−25.76 ± 6.91% vs. 39.52 ± 21.82%; $P < 0.01$; Fig. 4*B*).

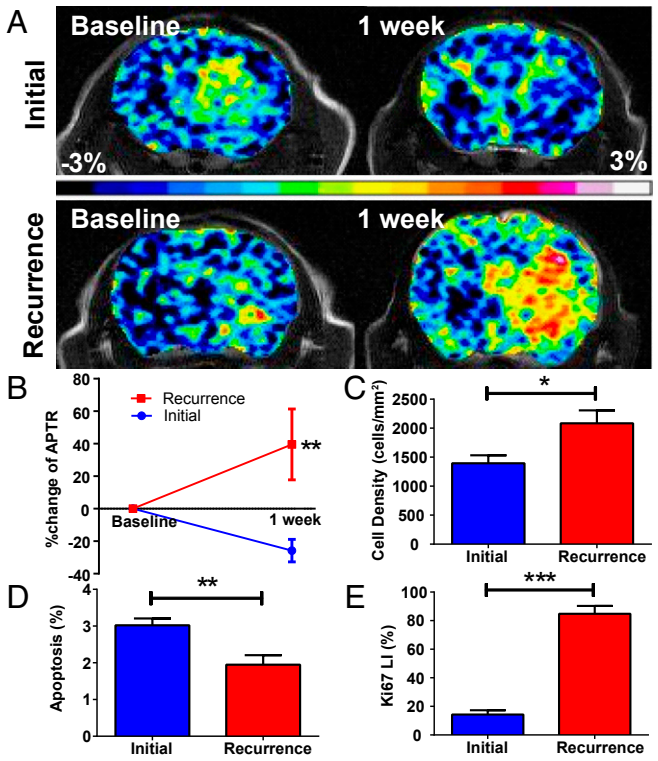

Fig. 4. Comparison between two tumor lines of glioblastoma from the same patient, one from initial resection and the other from the time of recurrence, which were clinically responsive and resistant to TMZ, respectively (experiment II). (*A*) Typical axial APTW images of brain in the initial (*Upper*) and recurrence (*Lower*) groups at baseline (*Left*) and 1 wk after (*Right*) treatment of TMZ. (*B*) The change (as a percentage) in the corrected APTR relative to baseline between the recurrence ($n = 6$) and the initial ($n = 3$) group. (*C*) Cell density between the two groups ($n = 3$ per group). (*D*) The percentage of cells showing apoptosis in the caspase-3 assay. (*E*) Ki67LI (i.e., percent of cells that are Ki67-positive). Data presented as mean ± SD (*$P < 0.05$, **$P < 0.01$, and ***$P < 0.0001$).

In the histological examination, the cell density was higher in the recurrent tumors (2,084 ± 224.0 /mm^2; $P < 0.05$) than in the initial tumors (1,395 ± 137.8 /mm^2) after one course of TMZ (Fig. 4*C*). In addition, the percentage of apoptotic cells was lower in the recurrent tumors (1.95 ± 0.26%; $P < 0.01$) than in the initial tumors (3.02 ± 0.19%; Fig. 4*D*). The Ki67LI in the recurrent tumors was markedly higher (84.76 ± 5.51%; $P < 0.0001$) compared with the initial tumors (14.25 ± 3.08%; Fig. 4*E*) after treatment. These results indicated that TMZ resistance was acquired through the development of the recurrent tumor from the initial tumor in the patient after a full course of radiation and TMZ. The results also indicated that APT signal does not decrease when the treatment is ineffective.

Discussion

TMZ is a second-generation alkylating agent currently considered the first choice for standard adjuvant treatment for GBM. It has been shown to improve survival significantly in newly diagnosed patients with GBM when used in combination with surgery and/or radiation (1, 5). However, recurrence is common even when the tumors respond well to initial therapy. This likely reflects development of TMZ resistance during adjuvant therapy (5, 7, 8). In radiological monitoring, it is difficult to assess tumor progression or treatment response because there are several types of treatment-related "reactions" that occur immediately to late after surgical resection or radiation therapy, especially concurrent with TMZ (24, 25). These tissue reactions, referred to as "pseudoprogression," have similar imaging characteristics as actual tumor, so it is difficult to differentiate between true tumor progression and pseudoprogression by use of conventional MR methods (26, 27). Thus, the neurooncology treatment team must rely on "best-guess" histories based on clinical context. Therefore, it is important to establish a method that might allow continuous monitoring of treatment response and/or recurrence in patients with glioma.

It is assumed that amide protons of endogenous mobile proteins and peptides in the cytoplasm are the major source of the APT signal (15). This was supported by an NMR study reporting that the amide protons of mobile protein/peptide side chains (Gln, Asn) and backbone amides resonate at 6.8 ppm and 8.2–8.4 ppm (2.1 ppm and 3.5–3.7 ppm downfield of water resonance) range, respectively (28). Zhou et al. demonstrated in two models of orthotopic murine glioma that APT imaging could clearly differentiate viable glioma (hyperintense) from radiation necrosis (hypointense to isointense), and that the APT signal of the tumor decreased substantially after radiation (19). That study supports the hypothesis that malignant gliomas have a higher concentration of endogenous mobile proteins and peptides than normal brain tissue or regions of radiation necrosis. The authors reported that their findings are consistent with an NMR proteomics report by Howe et al. (29), which showed that the tissue concentration of NMR detectable mobile proteins/peptides are higher in brain tumors than in normal white matter, and that they increase with tumor grade in the human brain. It is important to note in the study by Zhou et al. (19) that the reduced APT signal after radiation indicated a molecular tumor response that was detected earlier than with other commonly used MRI methods.

The present in vivo MRI study in HOT mouse GBM models tested whether APT imaging could detect a change in GBM amide-proton characteristics induced by short-term chemotherapy with TMZ. In experiment I, only one course of TMZ (3 d exposure and 4 d rest) at a dose of 80 mg/kg resulted in a substantial reduction in APT signal (Fig. 2*E*), although the tumor volume did not change detectably by conventional T2W imaging (Fig. 1). In all untreated control animals, the enhanced area and APT signal increased over the 1-wk period, indicating continued tumor growth. Histological examination of the tissue showed that short-term exposure to TMZ induced a marked reduction in Ki67LI by disturbance of DNA replication, but it did not show

any change in cell density, apoptosis rate, or observed morphology (Fig. 3). Consequently, the decreased total APT signal correlates with Ki67LI (Fig. S1*A*). This result suggests that the observed APT signal reflects production of endogenous mobile proteins and peptides specifically related to tumor proliferation. Therefore, we conclude that the decrease in APT signal observed in the treated group reflects proliferation arrest of tumor cells that respond to chemotherapy well before the tumor volume begins to decrease. Because molecular changes occur early in the time course of chemotherapy with TMZ and precede morphologic changes, the APT signal may serve as a useful, functional biomarker of the degree of tumor progression (malignancy) or treatment response.

In experiment II, the APT signal decreased in the initial tumor and increased in the recurrent tumor despite the same course of TMZ treatment in both groups, consistent with the clinical course in the patient, a response in the initial tumor, and progression in the recurrent tumor. The Ki67LI was substantially higher in the recurrent tumor. The data strongly suggest that APT signal is a sensitive imaging biomarker that can differentiate tumor progression from treatment effects and acquisition of TMZ resistance. Should this hold true in future studies, APT imaging has the potential to be an indispensable method for clinical management of patients with glioma.

One question of interest is the origin of the reduced APT signal after chemotherapy. To begin answering this question, the total protein content of tumors in untreated control vs. treated animals in experiment I were compared by using standard analytical protocols (30). In this study, total tumor protein was no different between the control and treated groups (66.28 ± 36.76 μg/mg tissue vs. 61.54 ± 14.77 μg/mg tissue; $P = 0.82$). This indicates that amount of the mobile protein/peptide components that contribute to the APT signal must be small in comparison with total protein. As it is known that abnormal proteosynthesis causes overexpression of various proteins or peptides in proliferation of tumor cells (31), it is not surprising that the APT signal correlated with the cell proliferation marker Ki67. Indeed, the present study, as well as earlier studies (18, 32), found correlations between the APT signal and Ki67LI. Another study demonstrated that positron emission tomography (PET) with the use of 3′-deoxy-3′-[^{18}F]fluorothymidine (FLT) PET, a noninvasive in vivo assessment of cell proliferation, could also assess tumor response to therapy (33). If APT imaging provides the same information as FLT PET provides, it is reasonable to hypothesize that APT imaging offers the detection of early response in the course of treatment. However, when one examines regional differences within a treated tumor in experiment I, Ki67LI was homogenously reduced over the tumor and, in particular, no differences in Ki67LI were found between regions showing an APT signal (Fig. S2, *Upper Right*) vs. regions in the same tumor where the APT signal had disappeared (Fig. S2, *Lower Right*). One possible explanation for this apparent discrepancy is that the excess abnormal proteins and peptides whose accumulation might be harmful to the cell (34) are usually degraded by intracellular proteolysis via lysosomal and ubiquitin–proteasome pathways (35). As the rates of degradation of individual cell constituents vary, with $t_{1/2}$ values ranging from 10 min to several days or weeks (35), the amount of protein degradation may vary by location within treated tumors, especially over a short 1-wk period after exposure to TMZ. Another possible contribution might be a reduction in intracellular pH after treatment with TMZ. This would also result in a decrease in APT signal because –NH proton exchange is known to be catalyzed by base (36). It is known that lysosomal proteolysis described earlier uses an H^+-ATPase pump in the membrane to generate acid, and, as the pH becomes more acidic (pH ~5), enzymes become activated (37). Although tumor cells produce a large amount of acid generated by glycolysis, they express various pH regulators, which actively increase proton efflux into the extracellular space to maintain an intracellular pH near neutral or slightly alkaline to avoid cell death (38). One could hypothesize that TMZ treatment disrupts pH regulation and that the intracellular pH becomes slightly more acidic in the treated tumors. In fact, it has been reported that intracellular acidification occurs in tumors during chemotherapy with an alkylating agent (39) or other types of agents (40–42). We postulate that reduction of tissue concentration of proteins/peptides in parallel with cellular acidification would contribute to the observed APT signal decrease as a tumor responds to chemotherapy with TMZ. A remaining question of interest is the identity of the endogenous proteins or peptides that contribute to the APT signal and their location within the tumor. To understand which specific biological events that underlie the change in a given APT signal, several other types of experimental models of tumorigenesis and sophisticated proteomics approaches will need to be investigated.

Although our present study was conducted by using a 7-T animal MRI scanner, the current clinical standard for high-field MRI scanners (3 T) would suffice for quantitative assessment of APT, as demonstrated in our previous study (18) and other studies (17, 43). It is known that CEST and APT should be enhanced at higher magnetic fields as a result of improved sensitivity and spectral resolution. Indeed, Smith et al. suggested that performing the APT imaging at 7 T might increase the ability to discern subtle changes (44) compared with APT imaging at 3 T. On the contrary, the APT signal is quite sensitive to field inhomogeneity (45), and this, plus possible limitation of specific absorption rate (46), may negate the positive attributes of high-field APT imaging in humans.

In conclusion, this study demonstrates that APT imaging was able to detect an early therapeutic response to TMZ and documents tumor progression in a model of TMZ resistance. The results suggest that APT imaging may serve as a useful biomarker for monitoring treatment response during chemotherapy and follow-up after treatment. APT imaging may detect early molecular metabolite changes that precede morphologic changes and cannot be detected with conventional MRI sequences. APT imaging as a molecular imaging tool does not require an endogenous contrast agent, and it is technically feasible with the use ofa standard clinical scanner (17, 43). Such technology could have a major impact on the clinical management of patients with glioma.

Materials and Methods

Animal Protocol. The animal protocols were approved by the institutional animal care and use committee, and the experiments were performed in accordance with the National Institutes of Health Guidelines on the Use of Laboratory Animals. The HOT mouse model of GBMs developed by Bachoo et al. were exploited (20, 21). Details of preparation of the model are provided in *SI Materials and Methods*.

MRI. Full details of MRI data acquisition are provided in *SI Materials and Methods*. Briefly, axial T2W/T1W images were obtained on a 7-T small-animal MR system to cover the entire brain with a fast spin-echo sequence. On a single 1-mm slice delineating the tumor, APT imaging was performed. Gradient echo images were obtained following a presaturation pulse (continuous-wave block pulse; B1, 2.3 μT; duration, 5 s), which was applied at 29 frequency offsets from 7 to −7 ppm with an interval of 0.5 ppm. A control image with the saturation offset at 300 ppm was also acquired.

MRI Data Analysis. All image data were analyzed with a program written in interactive data language (IDL; Research Systems) and ImageJ (version 1.44r; National Institutes of Health). First, the entire volume of the tumor on the T2W image was measured manually in the software. The T1W image was used as an aid for delineating tumor border. Second, the APTW image was processed. The definitions and terminology used in this study are equivalent to those in previous papers (15, 17, 47). The images obtained at 29 frequency offsets were first collected to obtain a *z*-spectrum. The *z*-spectrum was fitted on a pixel-by-pixel basis according to the procedure using the 12th-order polynomial fitting on positive and negative sides of frequency offsets, respectively, as previously reported (16, 17). Subsequently, the original *z*-spectrum was corrected pixel-wise for the any B_0 inhomogeneity through interpolation and centering of the *z*-spectrum. After the B_0 inhomogeneity correction, the APTW image was generated. APT is measured as a reduction in

bulk water signal as a result of chemical exchange of water protons with backbone amide protons of endogenous mobile proteins and peptides in tissue when a saturation pulse is applied at amide proton frequency of 3.5 ppm (downfield of water). However, the several saturation effects including direct water saturation and conventional magnetization transfer from semisolid tissue components or immobile macromolecules are observed after applying such a selective irradiation pulse (45). In an attempt to subtract out these effects, the APT signal is defined as the difference in tissue water intensity in images collected after presaturation at the amide proton frequency (+3.5 ppm with respect to the water proton MRI frequency) minus the water intensity after saturation at an equivalent upfield position (−3.5 ppm). Mathematically, the APTW image is defined as $[S(-3.5\text{ ppm}) - S(+3.5\text{ ppm})]/S(+300\text{ ppm})$, where S is the signal intensity on the images with presaturation pulse at each offset, assuming other signal contributions from the other saturation effects remain the same. Thus, the resulting APTW image represents the distribution of percent signal difference (APTR) between the images with presaturation pulse at +3.5 ppm and −3.5 ppm relative to reference image that was obtained with the saturation pulse at an extreme far offset (300 ppm) and expected to exclude any saturation effects.

In the quantitative analysis, APTW imaging was independently evaluated by two blinded observers. Regions of interest were carefully placed along the edge of the enhanced area (APTR $\geq -0.5\%$) on APTW image to measure area and APTR. APTR was also measured in contralateral normal appearing brain for a reference in each mouse. The corrected APTR was calculated as the difference between these two APTRs (i.e., tumor − normal). The values from the two observers were averaged to represent each animal.

Histological Examination. Four mice from each group in experiment I and three mice from each group in experiment II were killed and brains were harvested after the final MRI session for histological analysis. Pathologic slices were obtained in an axial plane corresponding to MR images and stained for H&E staining and Ki67 and caspase-3 immunohistochemical staining for microscopic examination. Total protein was also measured by using standard published protocols (30) in tumors from control and treated animals. Details of preparation and analysis are provided in *SI Materials and Methods*.

Statistical Analysis. All values are expressed as mean ± SD, and $P < 0.05$ is considered statistically significant. All statistical tests are detailed in *SI Materials and Methods*.

ACKNOWLEDGMENTS. The authors thank Drs. Shanrong Zhang, Ivan Dimitrov, Elena Vinogradov, and Robert Lenkinski for helpful discussions. This work was supported by Cancer Prevention and Research Institute of Texas Grant RP101243-P04-02 and National Institutes of Health Grants R01-CA115531 and P41-EB015908.

1. Stupp R, et al.; European Organisation for Research and Treatment of Cancer Brain Tumor and Radiotherapy Groups; National Cancer Institute of Canada Clinical Trials Group (2005) Radiotherapy plus concomitant and adjuvant temozolomide for glioblastoma. *N Engl J Med* 352(10):987–996.
2. Choi C, et al. (2012) 2-hydroxyglutarate detection by magnetic resonance spectroscopy in IDH-mutated patients with gliomas. *Nat Med* 18(4):624–629.
3. Thomas RP, Recht L, Nagpal S (2013) Advances in the management of glioblastoma: the role of temozolomide and MGMT testing. *Clin Pharmacol* 5:1–9.
4. Matsuda K, et al. (2012) Targeting JNK for therapeutic depletion of stem-like glioblastoma cells. *Sci Rep* 2:516.
5. Stupp R, et al.; European Organisation for Research and Treatment of Cancer Brain Tumour and Radiation Oncology Groups; National Cancer Institute of Canada Clinical Trials Group (2009) Effects of radiotherapy with concomitant and adjuvant temozolomide versus radiotherapy alone on survival in glioblastoma in a randomised phase III study: 5-year analysis of the EORTC-NCIC trial. *Lancet Oncol* 10(5):459–466.
6. Hegi ME, et al. (2005) MGMT gene silencing and benefit from temozolomide in glioblastoma. *N Engl J Med* 352(10):997–1003.
7. Mrugala MM, Chamberlain MC (2008) Mechanisms of disease: Temozolomide and glioblastoma—look to the future. *Nat Clin Pract Oncol* 5(8):476–486.
8. Johannessen TC, Bjerkvig R (2012) Molecular mechanisms of temozolomide resistance in glioblastoma multiforme. *Expert Rev Anticancer Ther* 12(5):635–642.
9. Wen PY, Kesari S (2008) Malignant gliomas in adults. *N Engl J Med* 359(5):492–507.
10. Waldman AD, et al.; National Cancer Research Institute Brain Tumour Imaging Subgroup (2009) Quantitative imaging biomarkers in neuro-oncology. *Nat Rev Clin Oncol* 6(8):445–454.
11. Fellner F, Fellner C, Held P, Schmitt R (1997) Comparison of spin-echo MR pulse sequences for imaging of the brain. *AJNR Am J Neuroradiol* 18(9):1617–1625.
12. van Zijl PC, Jones CK, Ren J, Malloy CR, Sherry AD (2007) MRI detection of glycogen in vivo by using chemical exchange saturation transfer imaging (glycoCEST). *Proc Natl Acad Sci USA* 104(11):4359–4364.
13. Mani T, et al. (2009) Modulation of water exchange in Eu(III) DOTA-tetraamide complexes: considerations for in vivo imaging of PARACEST agents. *Contrast Media Mol Imaging* 4(4):183–191.
14. Ren J, Trokowski R, Zhang S, Malloy CR, Sherry AD (2008) Imaging the tissue distribution of glucose in livers using a PARACEST sensor. *Magn Reson Med* 60(5):1047–1055.
15. Zhou J, Lal B, Wilson DA, Laterra J, van Zijl PC (2003) Amide proton transfer (APT) contrast for imaging of brain tumors. *Magn Reson Med* 50(6):1120–1126.
16. Salhotra A, et al. (2008) Amide proton transfer imaging of 9L gliosarcoma and human glioblastoma xenografts. *NMR Biomed* 21(5):489–497.
17. Zhou J, et al. (2008) Practical data acquisition method for human brain tumor amide proton transfer (APT) imaging. *Magn Reson Med* 60(4):842–849.
18. Togao O, et al. (2014) Amide proton transfer imaging of adult diffuse gliomas: correlation with histopathological grades. *Neuro-oncol* 16(3):441–448.
19. Zhou J, et al. (2011) Differentiation between glioma and radiation necrosis using molecular magnetic resonance imaging of endogenous proteins and peptides. *Nat Med* 17(1):130–134.
20. Marian CO, et al. (2010) The telomerase antagonist, imetelstat, efficiently targets glioblastoma tumor-initiating cells leading to decreased proliferation and tumor growth. *Clin Cancer Res* 16(1):154–163.
21. Marin-Valencia I, et al. (2012) Glucose metabolism via the pentose phosphate pathway, glycolysis and Krebs cycle in an orthotopic mouse model of human brain tumors. *NMR Biomed* 25(10):1177–1186.
22. Fisher ER, et al. (2002) Pathobiology of preoperative chemotherapy: findings from the National Surgical Adjuvant Breast and Bowel (NSABP) protocol B-18. *Cancer* 95(4):681–695.
23. McCluggage WG, et al. (2002) Morphological effects of chemotherapy on ovarian carcinoma. *J Clin Pathol* 55(1):27–31.
24. Brandsma D, Stalpers L, Taal W, Sminia P, van den Bent MJ (2008) Clinical features, mechanisms, and management of pseudoprogression in malignant gliomas. *Lancet Oncol* 9(5):453–461.
25. Hygino da Cruz LC, Jr., Rodriguez I, Domingues RC, Gasparetto EL, Sorensen AG (2011) Pseudoprogression and pseudoresponse: Imaging challenges in the assessment of posttreatment glioma. *AJNR Am J Neuroradiol* 32(11):1978–1985.
26. Fink J, Born D, Chamberlain MC (2011) Pseudoprogression: Relevance with respect to treatment of high-grade gliomas. *Curr Treat Options Oncol* 12(3):240–252.
27. Alexiou GA, et al. (2009) Glioma recurrence versus radiation necrosis: Accuracy of current imaging modalities. *J Neurooncol* 95(1):1–11.
28. van Zijl PC, et al. (2003) Mechanism of magnetization transfer during on-resonance water saturation. A new approach to detect mobile proteins, peptides, and lipids. *Magn Reson Med* 49(3):440–449.
29. Howe FA, et al. (2003) Metabolic profiles of human brain tumors using quantitative in vivo 1H magnetic resonance spectroscopy. *Magn Reson Med* 49(2):223–232.
30. Sambrook J, Fritsch EF, Maniatis T (1989) *Molecular Cloning: A Laboratory Manual* (Cold Spring Harbor Lab Press, Cold Spring Harbor, NY), 2nd Ed.
31. Cairns RA, Harris IS, Mak TW (2011) Regulation of cancer cell metabolism. *Nat Rev Cancer* 11(2):85–95.
32. Togao O, et al. (2013) Characterization of lung cancer by amide proton transfer (APT) imaging: An in-vivo study in an orthotopic mouse model. *PLoS ONE* 8(10):e77019.
33. Chen W, et al. (2007) Predicting treatment response of malignant gliomas to bevacizumab and irinotecan by imaging proliferation with [18F] fluorothymidine positron emission tomography: A pilot study. *J Clin Oncol* 25(30):4714–4721.
34. Rock KL, York IA, Saric T, Goldberg AL (2002) Protein degradation and the generation of MHC class I-presented peptides. *Adv Immunol* 80:1–70.
35. Burger AM, Seth AK (2004) The ubiquitin-mediated protein degradation pathway in cancer: Therapeutic implications. *Eur J Cancer* 40(15):2217–2229.
36. Zhou J, Payen JF, Wilson DA, Traystman RJ, van Zijl PC (2003) Using the amide proton signals of intracellular proteins and peptides to detect pH effects in MRI. *Nat Med* 9(8):1085–1090.
37. Hideshima T, Bradner JE, Chauhan D, Anderson KC (2005) Intracellular protein degradation and its therapeutic implications. *Clin Cancer Res* 11(24 pt 1):8530–8533.
38. Izumi H, et al. (2003) Cellular pH regulators: Potentially promising molecular targets for cancer chemotherapy. *Cancer Treat Rev* 29(6):541–549.
39. Affar B, Shah RG, Dallaire AK, Castonguay V, Shah GM (2002) Role of poly(ADP-ribose) polymerase in rapid intracellular acidification induced by alkylating DNA damage. *Proc Natl Acad Sci USA* 99(1):245–250.
40. Barry MA, Reynolds JE, Eastman A (1993) Etoposide-induced apoptosis in human HL-60 cells is associated with intracellular acidification. *Cancer Res* 53(10, suppl):2349–2357.
41. Goossens JF, Hénichart JP, Dassonneville L, Facompré M, Bailly C (2000) Relation between intracellular acidification and camptothecin-induced apoptosis in leukemia cells. *Eur J Pharm Sci* 10(2):125–131.
42. Nath K, et al. (2013) (31) P and (1) H MRS of DB-1 melanoma xenografts: Ionidamine selectively decreases tumor intracellular pH and energy status and sensitizes tumors to melphalan. *NMR Biomed* 26(1):98–105.
43. Wen ZB, et al. (2010) MR imaging of high-grade brain tumors using endogenous protein and peptide-based contrast. *Neuroimage* 51(2):616–622.
44. Klomp DW, et al. (2013) Amide proton transfer imaging of the human breast at 7T: Development and reproducibility. *NMR Biomed* 26(10):1271–1277.
45. Vinogradov E, Sherry AD, Lenkinski RE (2013) CEST: From basic principles to applications, challenges and opportunities. *J Magn Reson* 229:155–172.
46. Takahashi M, Uematsu H, Hatabu H (2003) MR imaging at high magnetic fields. *Eur J Radiol* 46(1):45–52.
47. Jones CK, et al. (2006) Amide proton transfer imaging of human brain tumors at 3T. *Magn Reson Med* 56(3):585–592.